Applied Catalysis B: Environmental 162 (2015) 470–474

Contents lists available at ScienceDirect

Applied Catalysis B: Environmental

journal homepage: www.elsevier.com/locate/apcatb

Selective transport of electron and hole among {0 0 1} and {1 1 0} facets of BiOCl for pure water splitting

Ling Zhang, Wenzhong Wang*, Songmei Sun, Dong Jiang, Erping Gao

State Key Laboratory of High Performance Ceramics and Superfine Microstructures, Shanghai Institute of Ceramics, Chinese Academy of Sciences, 1295 Dingxi Road, Shanghai 200050, PR China

ARTICLE INFO

Article history:
Received 2 April 2014
Received in revised form 11 July 2014
Accepted 13 July 2014
Available online 19 July 2014

Keywords:
Selective transport
Photo-deposition
BiOCl
Photocatalytic
Water splitting

ABSTRACT

The efficient spatial transport of photo-generated electrons and holes to different facets is critical to construct an efficient solar energy conversion system. BiOCl@Au/MnO_x hierarchical structure was fabricated by depositing the Au and MnO_x on the {0 0 1} and {1 1 0} crystal facets of BiOCl, respectively. The internal electric field (E_{IEF}) along the ⟨0 0 1⟩ direct, and strong local electric field (E_{LEF}) induced by the fast formed Au nanoparticles have been proposed as the intrinsic driving force for the spatial separation and transport of charge carriers in the BiOCl semiconductor, which resulted in significant enhancement of solar-driven photocatalytic activity for the pure water splitting without any sacrificial agent. The special structure of selective deposition of redox cocatalysts on the different facets of a single crystal should be promising and intriguing for designing highly efficient solar energy conversion photocatalyst.

1. Introduction

Separation and transport of photogenerated electrons (e^-) and holes (h^+) plays key roles in determining solar energy conversion efficiency of semiconductor-based photocatalyst. Efficient separation and transports of carriers to the crystal surface is a premise for the photocatalytic redox [1,2]. Finding the transport paths of carriers and identifying these active sites on the surface of photocatalyst are critical for improving the photocatalytic activity, especially in water splitting reactions. Therefore, an in-depth understanding on the mechanism of charge separation and transport to the active sites of semiconductors is necessary before constructing an efficient solar energy conversion system.

Photochemical labeling has been reported as an efficient way to obtain the information about charge separation in the irradiated semiconductor [3]. During the photochemical labeling process, catalyst powder was irradiated in the presence of precursors of different metal ions as well as some distinct electron donors/acceptors. Then the precursors were deposited on the surface of catalyst after a redox step. The locations of deposition were pinpointed as the redox-active sites for the semiconductors. Many research results have showed that the photo-generated electrons and holes would "selectively" reach on the different facets to take part in the photocatalysis separately [2,4]. However, not all of the photogenerated electrons and holes may be driven to different crystal facets of the semiconductor. There are few different experimental results that the photo-generated electrons and holes transported to the surface of the semiconductors without selectivity [3,5]. Those apparently contradictory results to some extent might confuse researchers on the essence of facets dependent charge separation: what is the intrinsic driving force for spatial transport of photo-generated electrons and holes to different facets? Thus, it remains a challenge to investigate internal relation between the selectively spatial charge separation and crystal structure of the semiconductors.

Here, we present evidences for the spatial separation of electrons and holes among the {0 0 1} and {1 1 0} crystal facets of BiOCl crystals under proper photo-deposition conditions. Different migration rates of the photo-generated electrons to {0 0 1} and {1 1 0} crystal facet resulted from the internal electric field (E_{IEF}) along the ⟨0 0 1⟩ direct, and strong local electric field (E_{LEF}) induced by the fast formed Au nanoparticles have been proposed as the intrinsic driving force for the spatial separation and transport of charge carriers in the BiOCl semiconductor based on the observed experimental phenomena. Furthermore, the recombination of photo-generated h^+ and e^- would be efficiently avoided due to the selective photo-deposition of Au and MnO_x on the {0 0 1} and {1 1 0} crystal facets of BiOCl, respectively. A significant

* Corresponding author. Tel.: +86 21 5241 5295; fax: +86 2152413122.
E-mail address: wzwang@mail.sic.ac.cn (W. Wang).

http://dx.doi.org/10.1016/j.apcatb.2014.07.024
0926-3373/

enhancement of photocatalytic activity for the pure water splitting was realized over the BiOCl@Au/MnO_x hierarchical structure without any sacrificial agent.

2. Experimental

2.1. Preparation of BiOCl photocatalysts terminated with {0 0 1} and {1 1 0} facets

BiOCl sample terminated with {0 0 1} and {1 1 0} facets was synthesized by a hydrothermal procedure according to a reported Ref. [6]. In a typical procedure, 2 mmol of $Bi(NO_3)_3{\cdot}5H_2O$ and 2 mmol of KCl were added in 30 mL distilled water at room temperature with continuous stirring. The mixture solution was stirred for 1 h and then poured into a 50 mL Teflon-lined stainless autoclave. The autoclave was allowed to be heated at 160 °C for 24 h, and then air cooled to room temperature. The resulting precipitates were collected and washed with ethanol and deionized water thoroughly and dried at 60 °C in air.

For the facets selective photo-depositions, three ways containing single reduction, single oxidation as well as simultaneous reduction and oxidation were carried out at room temperature without pH value adjusted (see in Table S1). Normally, 0.20 g BiOCl powder and designed amount of metal precursors (~4 wt%) were mixed in 200 ml deionized water. The cooling water jacket was set up to sustain the reaction temperature at 25 ± 0.5 °C. The suspension was then irradiated by a 500-W Xe lamp under continuous stirring. After 3 h photo-deposition, the suspension was filtered, washed with deionized water for several times, and finally dried at 60 °C overnight.

2.2. Characterizations

The samples were characterized by X-ray powder diffraction (XRD) on a Rigaku powder diffractometer. Each sample was scanned using Cu *K*α radiation with an operating voltage of 30 kV and an operating current of 100 mA. The scan rate of 4°/min was applied to record the patterns in the range of 10 – 70°. UV–vis diffuse reflectance spectra (DRS) were recorded on an UV–vis spectrophotometer (Hitachi H-3010) equipped with an integrating sphere. Chemical compositions of the derived products were analyzed using X-ray photoelectron spectroscopy (XPS) analysis (Thermo Scientific Escalab 250). All binding energies were referenced to the C 1s peak (285 eV) arising from adventitious carbon. The morphologies and microstructures of the as-prepared samples were investigated by transmission electron microscopy (TEM, FEI Tecnai G2 F30) and scanning electron microscopy (SEM, Hitachi S4800 and Hitachi 6700).

2.3. Preparation of photoelectrodes and electrochemical characterizations

As working electrode a thin film of as-prepared photocatalysts (BiOCl, BiOCl@Au, BiOCl@ MnO_x and BiOCl@Au/MnO_x, respectively) was deposited on a FTO conductive support (1.5 × 2 cm). A ethanol solution of Nafion (5%) containing about 20% as-prepared photocatalysts in weight was mixed and then spread on the FTO electrode. The film was allowed to air drying before heating in an oven at 80 °C for 30 min. The electrochemical characteristic of the as-prepared photoelectrodes were performed using CHI660D electrochemical work station. All the experiments were carried out within a three component cell. The as-prepared photoelectrodes were used as the working electrode, platinum wire was used as the counter electrode, and saturated calomel electrode (SCE) was used as the reference electrodes. The chopped current density of the electrodes were recorded at a scan rate of 5 mV s^{-1} over a voltage range of −0.4–1.4 V in 0.1 M Na_2SO_4 solution.

2.4. Water splitting by photocatalysis

The photocatalytic water splitting reactions were carried out in a closed gas circulation and evacuation system with a cooling water jacket to sustain the reaction temperature at 25 ± 0.5 °C and with a 500-W Xe lamp as light resource. Normally, 0.05 g photocatalyst was dispersed in 100 ml aqueous solution in a Pyrex reaction cell. Before irradiation, the reaction system was thoroughly degassed by N_2/Ar in order to drive off the air inside. The amount of evolved O_2 and H_2 were determined by an online gas chromatograph (Tianmei, GC-7890, TCD, N_2 or Ar carrier). The rate of evolution in the continue 6 h was recorded for comparison.

3. Results and discussion

3.1. Morphology and forming mechanism

The metals or metal oxide photo-depositions on the surface of BiOCl were obtained by using $HAuCl_4$ and $Mn(NO_3)_2$ as precursors without any scavenger. SEM images (Fig. 1a, b) clearly show that the Au and MnO_x particles are selectively photo-deposited on {0 0 1} and {1 1 0} facets of BiOCl single crystalline, respectively. The HAADF-STEM images and EDS analysis (Supplementary Fig. S1a,b) show the spatial distribution of the photo-deposits on the surface of the BiOCl. The XPS spectrum of Au 4f (Supplementary Fig. S2a) reveals that the deposited elements on the BiOCl are in metallic form with respect to the metal ion precursors. It indicates that the metal ions are photo-reduced on the {0 0 1} facets. On the other hand, two prominent peaks of Mn 2p (Supplementary Fig. S1b) at around 642 and 654 eV are due to the spin orbit splitting of 2p3/2 and 2p1/2 of Mn—O [7]. The broad peaks of Mn 2p3/2 and 2p1/2 in the spectrum indicate that Mn ion exists in several oxidation states [8]. Thus, Mn_3O_2 and Mn_3O_4 are considered to exist in a nonstoichiometric structure which is responsible for the amorphous structure of MnO_x (Supplementary Fig. S3). Namely, the photogenerated electrons and hole are readily available for the oxidation reaction on the {0 0 1} facets and reduction reaction on the {1 1 0} facets of BiOCl, respectively.

However, is it really that the photogenerated electrons and holes would intrinsically spatial transport to the {0 1 0} and {1 1 0} facets of BiOCl, respectively? Following experimental result gives a negative answer. The sponge-like MnO_x, from photo-reduction of Mn^{7+} ($KMnO_4$) or photo-oxidation of Mn^{2+} ($Mn(NO_3)_2$), were deposited all over the BiOCl surface (Supplementary Fig. S4). It indicates that the photogenerated carriers would not intrinsically and spatially transport to the different facets of BiOCl. The Mn^{7+} photo-reduction depositions occur all over the surface of the BiOCl which means that the photogenerated electron in the conduction band (CB) randomly moves to the surface to bring about the photoreduction. On the other hand, Mn^{2+} photo-oxidation deposits were also found all over the surface which indicates that the photo-generated hole in the valence band (VB) could transfer to the surface of the photocatalyst without selectivity. In the BiOCl crystal, the VBM is mainly contributed to O2p and Cl2p states, and the Bi6p states dominate the CBM [9]. The photogenerated electron will move at the 6p orbital conduction band of the Bi^{3+} in the $[Bi_2O_2]_2^{2+}$ slab of the particles, while the photogenerated hole will exist at the 2p orbital of O^{2-} or Cl^- at the crystal surface. According to the band structures and atom arrangement of {0 0 1} and {1 1 0} facets (Supplementary Fig. S5), the photo-generated electron and hole are accessible throughout the surface of BiOCl particles. As a result, the manganese oxide

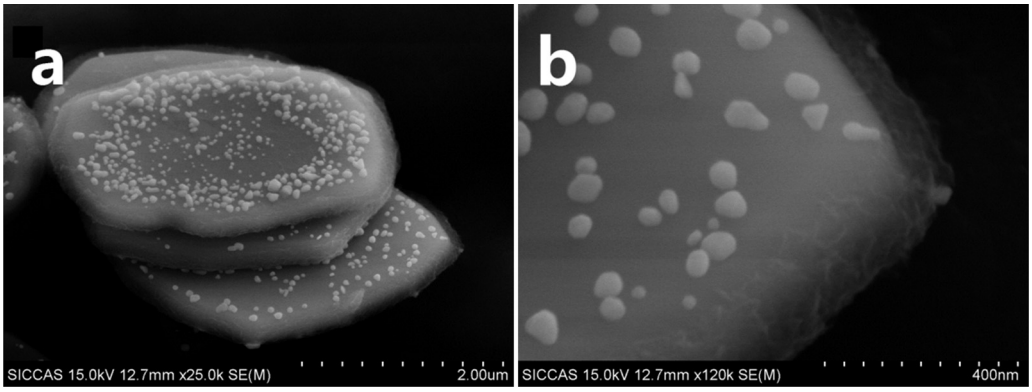

Fig. 1. (a) SEM images of BiOCl@Au/MnO_x; (b) enlarged SEM image.

deposited from photo–reduction or oxidation has been found all over the surface of BiOCl.

The photo-depositions of metals on the surface of BiOCl had carried out using $HAuCl_4$ (or $AgNO_3$, H_2PtCl_6) as precursors and water (or methanol) as holes scavenger. It clearly shows that the Au or Ag nanoparticles (although with different particle sizes) are deposited on the {0 0 1} facets of BiOCl (Supplementary Figs. S6 and S7). However, the Pt particles were found on the surface of the BiOCl only when the methanol as the holes scavenger since the Pt (IV) is hard to be photo-reduced to Pt (0) in pure water. We presume the selective electron transport to the {0 0 1} facets could be resulted from the following reasons: first, the mobility of photo-generated electrons to the {0 0 1} facets was the fastest among all facets due to an internal electronic filed (E_{IEF}) along the *c*-axis [10–12]. Furthermore, for the square plate of the as-prepared BiOCl, the mean diffusion paths to the {0 0 1} facets is shorter than that of {1 1 0} facets since the thickness (about 200–300 nm) of the plates is smaller that of the width (about 1–2 μm). Thus, the electrons would fast diffuse to {0 0 1} facets to reduce the metal ions. Sequentially, these formed metal nanoparticles irradiated under their plasmon resonance frequency can generate intense local electric fields near the surface of the nanoparticles. This plasmonic local electric field (E_{LEF}) helps the formation of an electric filed inside the semiconductor that could help 'pull' electrons and holes apart [13]. The formed Au or Ag nanoparticles also usually act as an "electron sink" for photo-generated electrons in semiconductors [14]. Finally, the photo-generated electrons in the semiconductor preferentially transfer from the conduction band to these metal nanoparticles deposited on the {0 0 1} facets of BiOCl. On the other hand, the adsorption effect originating from the precursor ions and preparative environments should be considered. Au^{3+}/Ag^{+} ions would prior absorb on the {0 0 1} facets due to the electrostatic force (especially when the {0 0 1} facets were terminated with the Cl^{-} ions). It has been proved that the Au nanoparticles were preferentially formed on the {0 0 1} facets even the gold was reduced by sodium citrate in the aqueous solution (Supplementary Fig. S6b).

When the $HAuCl_4$ and $Mn(NO_3)_2$ used as precursors to simultaneously proceed the photo-depositions reaction, as shown in Fig. 2a, first, the Au nanoparticles with diameter of 20–30 nm were found on the {0 0 1} facets of BiOCl (30s), but the MnO_x was hard to be found in the TEM image. After 60 s of light irradiation, the MnO_x emerged on the side of BiOCl single crystal (Fig. 2b). With the irradiation time increasing to 300 s, the thickness of the MnO_x increased to 60–80 nm. These results suggested the photoreduction reaction of Au^{3+} to metal nanoparticles occurred antecedent to the photooxidation reaction of MnO_x. Now, based on the observed experimental phenomena, we draw several possible reasons to explain the "selectively" spatial transport of photo-generated carriers between the {0 0 1} and {1 1 0} facets of the BiOCl (as shown in Scheme 1a): (1) the photoexcitation of BiOCl with photons with energy larger than the bandgap leads to the generation of electrons in the semiconductor conduction band and electron holes in the valence band. The photo-generated electron diffused to the {0 0 1} prior to that of hole and other facets since the "inner electric filed" along the *c*-axis and the shorter thickness of the as-prepared BiOCl plates. The formed Au nanoparticles on the {0 0 1} facets, as reservoirs, selectively "pulled out" more photogenerated electrons to these active sites and reduce the Au^{3+} to metal under the help of E_{ple}. (2) Some of "valid" photo-generated holes diffused to the {1 1 0} facets to complete the photo-oxidation of Mn^{2+}, but some "invalid" holes transferred to the {0 0 1} facets where they were recombined with the electrons quickly. As an experimental phenomenon, the selective photo-reduction of metal and photo-oxidation of metal oxidation were observed on the {0 0 1} and {1 1 0} facet of BiOCl, respectively.

3.2. Photoelectrochemical process and photocatalytic water splitting

When the light continually irradiated the photo-deposited BiOCl sample, the photo-generated electrons and holes would "selectively" transported to the Au nanoparticles on the {0 0 1} facets and the MnO_x on the {1 1 0} facets, respectively (as shown in Scheme 1b). This apparent phenomenon that the electron transport to Au nanoparticles and hole transported on the MnO_x during the illumination will be advantageous for the photocatalytic water splitting, because that the Au nanoparticles and the nanostructured MnO_x ($Mn^{III,IV}$) were helpful for photoelectrochemical water splitting [15–18]. That is to say, the two redox functional components spatially separated in the as-prepared BiOCl@Au/MnO_x hierarchical structure, and the photo-generated carriers would "selectively" transport to these sites.

Four typical electrodes, denoted as BiOCl, BiOCl@Au, BiOCl@MnO_x and BiOCl@Au/MnO_x, have been prepared to examine the electrochemical overpotentials of the catalysts for water oxidation and water reduction. Potential and current scans of the as-prepared electrodes in 0.1 M Na_2SO_4 solution are shown in Fig. 3. Under these conditions, the proton reduction potentials occur in the following order: BiOCl@MnO_x > BiOCl > BiOCl@Au > BiOCl@Au/MnO_x; that is, the BiOCl@Au/MnO_x possesses the highest ability of reducing protons. The deposition of Au cocatalysts is advantageous for moving the proton reduction overpotentials to lower values. However, water oxidation potentials show different trend: BiOCl@MnO_x < BiOCl@Au/MnO_x < BiOCl@Au < BiOCl; that is, the BiOCl@MnO_x possesses the highest ability of oxidizing water. MnO_x attachment does reduce the overpotentials slightly. Given that MnO_x is a well-known water oxidation catalyst [16–19], this

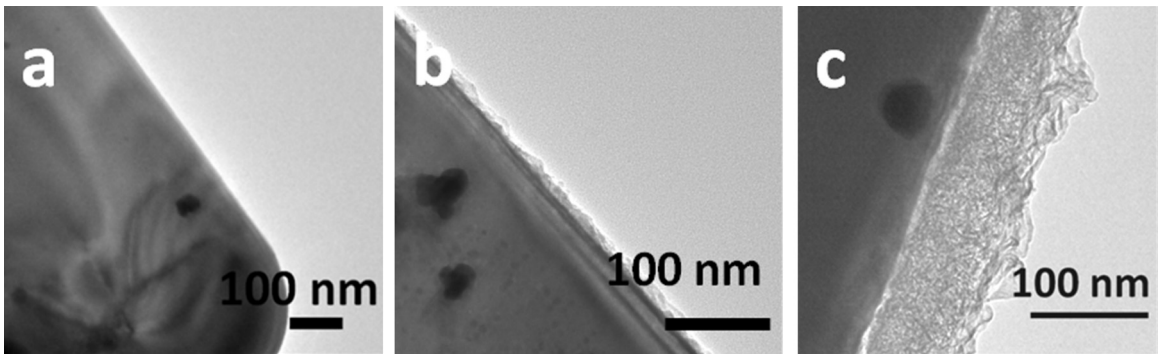

Fig. 2. TEM images of BiOCl nanoplates photodeposited under Xe lamp illumination: (a) for 30 s; (b) for 60 s; (c) for 300 s.

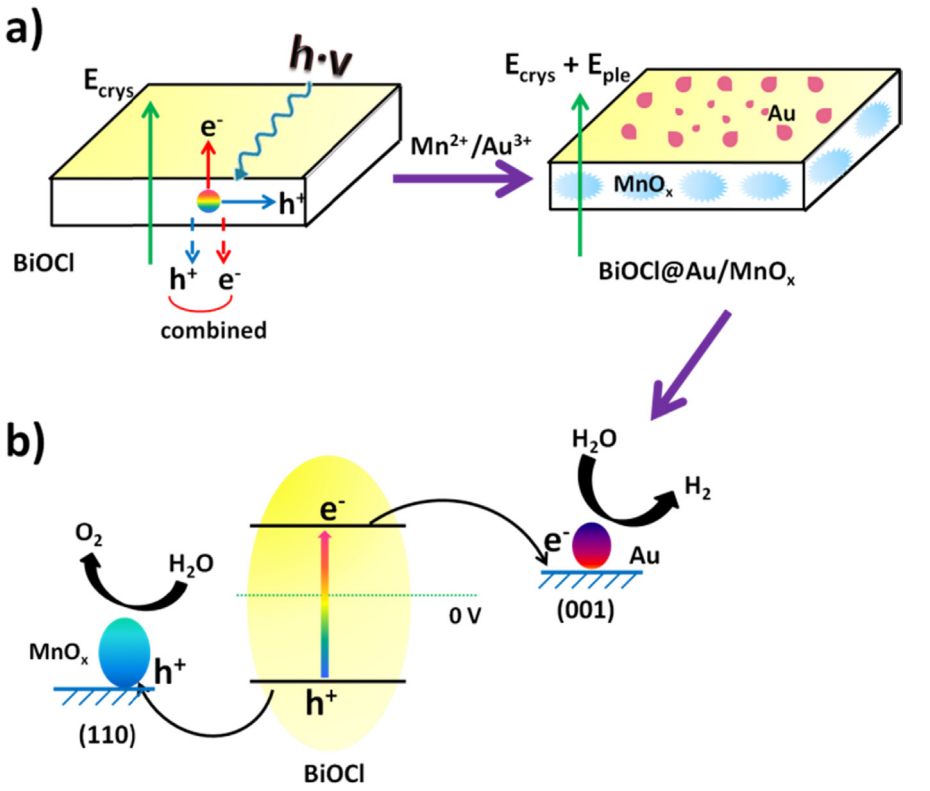

Scheme 1. (a) Selective photo-deposition on BiOCl: photo-reduction deposition of Au metals on the {0 0 1} facet and photo-oxidation deposition of MnO_x on the {1 1 0} facet. (b) Elementary steps occurring in the photocatalytic oxygen evolution upon irradiation of BiOCl@Au/MnO_x with Xe lamp.

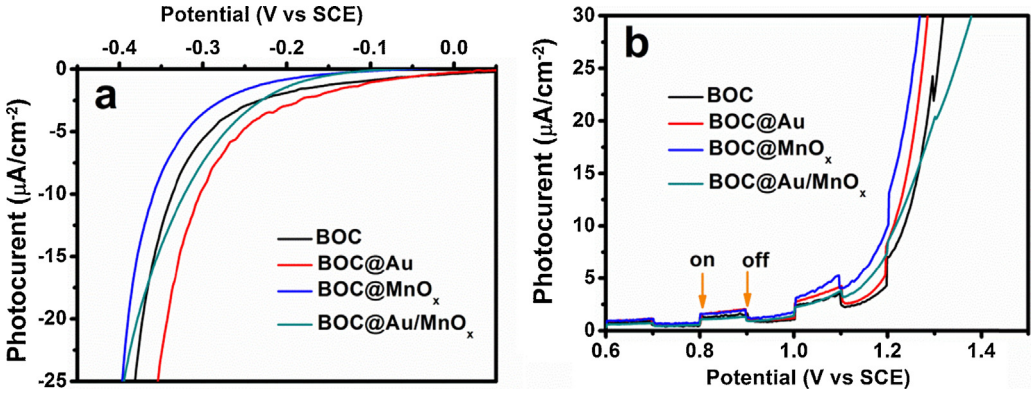

Fig. 3. Photochemical performances of four as-prepared photoelectrodes. Reaction conditions: 0.1 M Na_2SO_4 aqueous solution. Light source, 500 W Xe lamp, Scan rate: 5 mV s^{-1}. The light was chopped during the anodic sans.

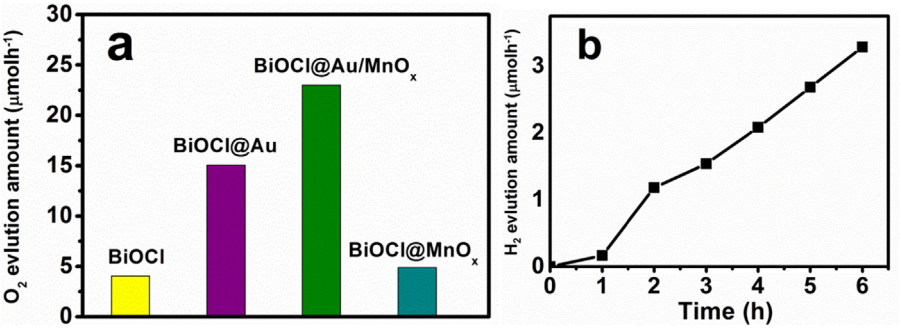

Fig. 4. (a) O_2 evolution upon Xe lamp irradiation of an aqueous suspension containing: BiOCl, BiOCl@Au, BiOCl@ MnO_x and BiOCl@Au/MnO_x, respectively. The gas phase was evacuated at every for 6 h of reaction and the amount of evolved O_2. (b) H_2 evolution upon Xe lamp irradiation of an aqueous suspension containing BiOCl@Au/MnO_x. Reaction conditions: photocatalyst 0.05 g; H_2O 100 mL; 500 W Xe lamp; an inner irradiation type quartz cell.

result indicated that MnO_x loading promoted water oxidation on BiOCl.

In order to further illustrate the function of the deposits, the four as-prepared samples (BiOCl, BiOCl@Au, BiOCl@ MnO_x and BiOCl@Au/MnO_x) were evaluated by the photocatalytic water splitting reactions. As shown in Fig. 4a, the photocatalytic oxygen evolution activity is strongly dependent on the species of the photo-deposits. The highest water oxidation activity is achieved for the BiOCl@Au/MnO_x sample. This result indicates that when the reduction/oxidation cocatalysts are selectively deposited on the appropriate facets, the photocatalytic performance can be most greatly enhanced. Furthermore, the BiOCl is usually self-reduced by the photo-generated e^- which resulted in the photocorrosion [20,21]. In this study, we found that the oxygen evolution rate of the BiOCl@MnO_x was very high at the initial stage but it would drop down along with the irradiation time (Supplementary Fig. S8a). However, the oxygen evolution rate of the BiOCl@Au/MnO_x sample was stable during a 30 h irradiation (Supplementary Fig. S8b). It means that photo-generated e^- would be transfer to the Au nanoparticles and the self-reduction of Bi3+ to Bi was avoided. It is worth to note, that constant increase of H_2 was detected only when the BiOCl@Au/MnO_x sample as the photocatalyst (Fig. 4b), but a trace of H_2 was detected when the BiOCl@Au sample in the pure water. The O_2 and H_2 evolution amount were increased with the increasing of the content of Au and MnO_x deposits (Supplementary Table S2). Furthermore, the amount of the H_2 was much smaller than that of the O_2 produced in the photocatalysis. It means there are competitive reactions consuming the photo-generated electrons. This question is currently under investigation in the laboratory.

4. Conclusions

In summary, the BiOCl@Au/MnO_x hierarchical structure was obtained by depositing the Au and MnO_x on the {0 0 1} and {1 1 0} crystal facets of BiOCl, respectively. The nature driving force for the "selectively" spatial transport is mainly owing to the internal electronic filed (E_{IEF}) along the C-axis in the BiOCl crystal, and local electric field (E_{LEF}) induced by the fast formed Au nanoparticles on the {0 0 1} facets. The "selective" transport of electron and hole to different facets would be advantageous for realizing and enhancing the photocatalytic water splitting. The selective deposition of redox cocatalysts on the different facets of a single crystal, and efficient charge separation between different facets should be promising and intriguing for designing highly efficient solar energy conversion system.

Acknowledgements

This work was supported by 973 Program (2013CB933203) and the National Natural Science Foundation of China (51272303 and 50972155). This work was financially supported by the National Basic Research Program of China (Grant Nos. 2013CB933203, 51272303 and 50972155)

Appendix A. Supplementary data

Supplementary material related to this article can be found, in the online version, at http://dx.doi.org/10.1016/j.apcatb.2014.07.024.

References

[1] A.V. Akimov, A.J. Neukirch, O.V. Prezhdo, Chem. Rev. 113 (2013) 4496–4565.
[2] R. Li, F. Zhang, D. Wang, J. Yang, M. Li, J. Zhu, X. Zhou, H. Han, C. Li, Nat. Commun. 4 (2013) 1432.
[3] E.M. Sabio, M.F. Chi, N.D. Browning, F.E. Osterloh, Langmuir 26 (2010) 7254–7261.
[4] T. Ohno, K. Sarukawa, M. Matsumura, New J. Chem. 26 (2002) 1167–1170.
[5] G.H. Dong, L.Z. Zhang, J. Phys. Chem. C 117 (2013) 4062–4068.
[6] J. Jiang, K. Zhao, X. Xiao, L. Zhang, J. Am. Chem. Soc. 134 (2012) 4473–4476.
[7] S.L. Chou, F.Y. Cheng, J. Chen, J. Power Sources 162 (2006) 727–734.
[8] Y. Huo, H. Zhang, J. Jiang, Y. Yang, J. Mater. Sci. 47 (2012) 7026–7034.
[9] L. Zhao, X. Zhang, C. Fan, Z. Liang, P. Han, Phys. B: Condens. Matter 407 (2012) 3364–3370.
[10] H. Zhang, L. Liu, Z. Zhou, RSC Adv. 2 (2012) 9224.
[11] X. Lin, Z. Shan, K. Li, W. Wang, J. Yang, F. Huang, Solid State Sci. 9 (2007) 944–949.
[12] J. Li, L. Zhang, Y. Li, Y. Yu, Nanoscale 6 (2014) 167.
[13] X. Zhang, Y.L. Chen, R.-S. Liu, D.P. Tsai, Rep. Prog. Phys. 76 (2013) 046401.
[14] A. Primo, T. Marino, A. Corma, R. Molinari, H. Garciía, J. Am. Chem. Soc. 133 (2011) 6930–6933.
[15] A. Kubacka, M. Fernández-García, G. Colón, Chem. Rev. 112 (2012) 1555–1614.
[16] D.M. Robinson, Y.B. Go, M. Mui, G. Gardner, Z. Zhang, D. Mastrogiovanni, E. Garfunkel, J. Li, M. Greenblatt, G.C. Dismukes, J. Am. Chem. Soc. 135 (2013) 3494–3501.
[17] A. Primo, A. Corma, H. García, Phys. Chem. Chem. Phys. 13 (2011) 886.
[18] G. Liu, L.Z. Wang, H.G. Yang, H.M. Cheng, G.Q. Lu, J. Mater. Chem. 20 (2010) 831–843.
[19] Z.H. Ai, S.C. Lee, Y. Huang, W.K. Ho, L.Z. Zhang, J. Hazard. Mater. 179 (2010) 141–150.
[20] S. Weng, B. Chen, L. Xie, Z. Zheng, P. Liu, J. Mater. Chem. A 1 (2013) 3068.
[21] J. Jiang, L.Z. Zhang, H. Li, W.W. He, J.J. Yin, Nanoscale 5 (2013) 10573–10581.